IEEE Trans. on Medical Imaging 19:10 (2000) 1-11

# Biomechanical modeling of the human head for physically-based, non-rigid image registration

A. Hagemann[1], K. Rohr[1], H. S. Stiehl[1], U. Spetzger[2], J. M. Gilsbach[2]

*Abstract*— **The accuracy of image-guided neurosurgery generally suffers from brain deformations due to intraoperative changes. These deformations cause significant changes of the anatomical geometry (organ shape and spatial inter-organ relations) thus making intraoperative navigation based on preoperative images error-prone. In order to improve the navigation accuracy, we developed a biomechanical model of the human head based on the finite element method, which can be employed for the correction of preoperative images to cope with the deformations occurring during surgical interventions. At the current stage of development, the two-dimensional (2D) implementation of the model comprises two different materials, though the theory holds for the three-dimensional (3D) case and is capable of dealing with an arbitrary number of different materials. For the correction of a preoperative image, a set of homologous landmarks has to be specified which determine correspondences. These correspondences can be easily integrated into the model and are maintained throughout the computation of the deformation of the preoperative image. The necessary material parameter values have been determined through a comprehensive literature study. Our approach has been tested for the case of synthetic images and yields physically plausible deformation results. Additionally, we carried out registration experiments with a preoperative MR image of the human head and a corresponding postoperative image simulating an intraoperative image. We found, that our approach yields good prediction results, even in the case when correspondences are given in a relatively small area of the image only.**

*Keywords*— **Elasticity theory, biomechanical model, inhomogeneous materials, finite element method, intraoperative image correction**

## I. Introduction

THE accuracy of image-guided neurosurgery generally suffers from intraoperative brain deformations caused by brain shift or tumor resection, which may result in rather large changes in the geometrical and spatial organization of the brain, see, e.g., Hill *et al.* [1] or Maurer *et al.* [2]. To improve upon navigation accuracy, we developed a biomechanical model of the human head which allows to predict intraoperative brain deformations and thus to correct a preoperative image with respect to surgery-induced effects.

Recent work in the field of intraoperative image correction comprises different models of the human head, each of which allows to incorporate anatomical structures with spatially *variable material properties*. Some of these head models are based on physical motivations only, e.g., mass-spring systems [3] or combined energy terms [4]. However, these types of models do not incorporate real physical material parameters and hence are only weakly related to the physical behaviour of biological soft tissue. In contrast to these physically motivated models, other approaches are based on a direct physical description of the material behaviour.

One approach is the model of Davatzikos [5], where linear elasticity theory is used as a physical basis. Additional terms for modelling material inhomogeneities were introduced into the equilibrium description of the underlying linear elastic body. The resulting equations were then solved by successive overrelaxation. Despite the general difficulty to accurately determine the required external forces from images, Davatzikos applied image-derived forces to drive the deformation of the linear elastic body. As material parameter values, the author used heuristic values. More recently, another approach has been developed by Kyriacou and Davatzikos [6]. For the simulation of incompressible materials, a variation of the Mooney-Rivlin strain energy function [7], [8] has been applied, leading to a so called neo-Hookean material [9]. However, the used strain energy function equals the Mooney-Rivlin strain energy function only if the second Mooney-Rivlin parameter is set to zero which is in contrast to the value determined, and compared against reported measurements [10] by Mendis *et al.* [8]. The resulting equations are solved by the finite element method. Instead of explicitly modelling different anatomical structures, the authors introduced appropriate boundary conditions resulting from the assumptions that, e.g., the dura mater is non-moving (known as *homogeneous Dirichlet boundary condition*) and that no movement occurs between the dura mater and the brain at the contact surface (the so called *no-slip boundary condition*). The model of Lester *et al.* [11] is based on an inhomogeneous viscous fluid model described by modified Navier-Stokes equations, with locally varying viscosity parameters for the simulation of different anatomical structures. As above, forces were used to drive the deformation and the resulting equations are solved by successive overrelaxation. An apparent problem with this model is the assumption that all brain structures behave like a viscous fluid which is evidently not the case. Škrinjar *et al.* [12] used a set of mass nodes connected by Kelvin models to simulate the deformation behaviour of brain tissue. A Kelvin model is a simplified mechanical model of viscosity [13], [14] and consists of a parallel connection of a linear spring and a

[1]Universität Hamburg, FB Informatik, AB Kognitive Systeme, Vogt-Kölln-Straße 30, D-22527 Hamburg, Germany Tel.: +49 (40) 42883 2577 Fax: +49 (40) 42883 2572 E-Mail: hagemann@informatik.uni-hamburg.de

[2]Neurochirurgische Klinik, Universitätsklinik der Rheinisch-Westfälischen Technischen Hochschule (RWTH), Pauwelstraße 30, D-52057 Aachen, Germany

dashpot. The deformation is driven by applied forces and different anatomical structures are modeled by appropriate boundary conditions only. Paulsen *et al.* [15] modified a previously proposed approach of Tada *et al.* [16] such as to deal with subsurface brain deformation. The approach is based on consolidation theory and the finite element method is used to solve the underlying differential equations. In consolidation theory, the brain is regarded as a biphasic system represented by an elastic matrix and an interstitial fluid. Different material properties are introduced by spatially varying material parameter values as well as by applying appropriate boundary conditions. The deformation is driven by inhomogeneous Dirichlet boundary conditions only, i.e., in this case the deformation is prescribed at the brain surface.

Our approach is based on the well-established physical theory of continuum mechanics to handle inhomogeneous materials (see [17] for an earlier version). We apply the conforming finite element method for discretization, resulting in a large linear matrix system. Instead of using forces, which are generally difficult to be accurately determined from images, we use a set of given correspondences to drive the deformation of the preoperative image. According to the respective underlying anatomical structure, different materials are incorporated through physically connecting homogeneous subregions by appropriate boundary conditions. The necessary material parameter values were determined through a comprehensive literature study. Prior to our registration experiments with clinical pre- and postoperative MR images, we carried out experiments with synthetic images in order to assess the physical plausibility of the deformations predicted by our model.

## II. Approach

Our biomechanical model is based on the *equilibrium equations*, which describe the deformation of a body $\Omega$ under externally applied forces,

$$\begin{cases} -\operatorname{div}\boldsymbol{\sigma} = \mathbf{f} & \text{in } \Omega, \\ \boldsymbol{\sigma}\,\mathbf{n} = \mathbf{g} & \text{on } \Gamma, \end{cases} \tag{1}$$

where $\boldsymbol{\sigma}$ denotes the *Eulerian stress tensor*, $\mathbf{f}$ the applied body forces, $\mathbf{n}$ the unit vector normal to the surface $\Gamma$, and $\mathbf{g}$ the forces acting on $\Gamma$. To incorporate material properties of $\Omega$, the appropriate *constitutive equation*, which describes the stress/strain relationship of the body, has to be substituted into the equilibrium equations. Despite the known specialized constitutive equations for biological tissues like, e.g., brain tissue [13], [8], [18], Hooke's law

$$\boldsymbol{\sigma} = \lambda(\operatorname{tr}\mathbf{e}(\mathbf{u}))\mathbf{I} + 2\mu\mathbf{e}(\mathbf{u}) \tag{2}$$

is used in our model so far. This choice is motivated by the fact, that most biological tissues behave as a linear elastic material in the case of small strains [19], [14] which are implicitly assumed by using the Eulerian stress tensor $\boldsymbol{\sigma}$. After the substitution of Hooke's law, the equilibrium equations read

$$\begin{cases} -\operatorname{div}[\lambda(\operatorname{tr}\mathbf{e}(\mathbf{u}))\mathbf{I} + 2\mu\mathbf{e}(\mathbf{u})] = \mathbf{f} & \text{in } \Omega \\ (\lambda(\operatorname{tr}\mathbf{e}(\mathbf{u}))\mathbf{I} + 2\mu\mathbf{e}(\mathbf{u}))\mathbf{n} = \mathbf{g} & \text{on } \Gamma. \end{cases} \tag{3}$$

Here, $\lambda$ and $\mu$ denote the common *Lamé constants*, $\mathbf{u}$ the unknown displacement vector field, $\mathbf{e}(\cdot)$ *Cauchy's infinitesimal strain tensor*, $\mathbf{I}$ the identity matrix, and $(\operatorname{tr}\cdot)$ the trace operator.

In order to solve the equations of motion for the unknown function $\mathbf{u}$ assumed to lie within a sufficiently smooth function space, we use the *method of weighted residuals* [20], [21]. With this method, we demand that the projection of the residual onto arbitrary weighting functions $\mathbf{w}$ of the function space vanishes over the body $\Omega$:

$$\int_\Omega \langle -\operatorname{div}[\lambda(\operatorname{tr}\mathbf{e}(\mathbf{u}))\mathbf{I} + 2\mu\mathbf{e}(\mathbf{u})] - \mathbf{f}, \mathbf{w}\rangle \, d\Omega = 0, \tag{4}$$

with $\langle\cdot,\cdot\rangle$ denoting the common inner product. After some calculus, this can be transformed into

$$\int_\Omega \lambda(\operatorname{tr}\mathbf{e}(\mathbf{u}))(\operatorname{tr}\mathbf{e}(\mathbf{w})) + 2\mu\langle\mathbf{e}(\mathbf{u}),\mathbf{e}(\mathbf{w})\rangle \, d\Omega = \int_\Omega \langle\mathbf{f},\mathbf{w}\rangle \, d\Omega + \int_\Gamma \langle\mathbf{g},\mathbf{w}\rangle \, d\Gamma. \tag{5}$$

Through application of the *Galerkin method*, i.e. using only a finite dimensional subspace spanned by a finite number of basis functions $\boldsymbol{\phi}_i$, we can approximate the function $\mathbf{u}$ by a finite sum of basis functions $\boldsymbol{\phi}_i$ multiplied with unknown coefficients $u_i$,

$$\mathbf{u} = \sum_i u_i \boldsymbol{\phi}_i. \tag{6}$$

Substitution of this approximation into (5) and choosing a weighting function $\mathbf{w}$ represented by $\sum_j \boldsymbol{\phi}_j$, leads to the expression

$$\sum_i u_i \int_\Omega \lambda(\operatorname{tr}\mathbf{e}(\boldsymbol{\phi}_i))(\operatorname{tr}\mathbf{e}(\boldsymbol{\phi}_j)) + 2\mu\langle\mathbf{e}(\boldsymbol{\phi}_i),\mathbf{e}(\boldsymbol{\phi}_j)\rangle \, d\Omega = \int_\Omega \langle\mathbf{f},\boldsymbol{\phi}_j\rangle \, d\Omega + \int_\Gamma \langle\mathbf{g},\boldsymbol{\phi}_j\rangle \, d\Gamma, \tag{7}$$

which can be written in compact matrix notation as

$$\mathbf{A}\mathbf{u} = \mathbf{f} + \mathbf{g}, \tag{8}$$

where the matrix $\mathbf{A}$ is commonly known as *stiffness matrix*.

So far, the derived linear equation system (8) contains the description of a *homogeneous*, linear elastic body only. By dividing an inhomogeneous body $\Omega$ into a set of homogeneous subregions $\Omega_i$ according to the underlying anatomical structures, we are able to simulate *inhomogeneous* material behaviour with our model. Therefore, all subregions $\Omega_i$ are physically linked by the *compatibility* and *equilibrium* boundary conditions [14], [21]. The former condition states, that the displacements $\mathbf{u}_\Gamma^{ij}$ along the common

boundary $\Gamma_{ij}$ between two subregions $\Omega_i$ and $\Omega_j$ must be equal, while the latter one states that in the equilibrium, the sum of all stress vectors acting on the boundary $\Gamma_{ij}$ must be zero. These boundary conditions, while assuming homogeneous body forces $\mathbf{f}$ over $\Omega_i \cup \Omega_j$, allow us to couple both linear systems, yielding one linear equation system for the composite body $\Omega$:

$$\underbrace{\begin{pmatrix} \mathbf{A}_{11}^i & \mathbf{A}_{1\Gamma}^i & \mathbf{0} \\ \mathbf{A}_{\Gamma 1}^i & \mathbf{A}_{\Gamma\Gamma}^i + \mathbf{A}_{\Gamma\Gamma}^j & \mathbf{A}_{\Gamma 1}^j \\ \mathbf{0} & \mathbf{A}_{1\Gamma}^j & \mathbf{A}_{11}^j \end{pmatrix}}_{\mathbf{A}} \underbrace{\begin{pmatrix} \mathbf{u}^i \\ \mathbf{u}_\Gamma^{ij} \\ \mathbf{u}^j \end{pmatrix}}_{\mathbf{u}} = \underbrace{\begin{pmatrix} \mathbf{f} + \mathbf{g}^i \\ \mathbf{f} \\ \mathbf{f} + \mathbf{g}^j \end{pmatrix}}_{\mathbf{b}}. \quad (9)$$

With $\mathbf{A}_{11}^i$ etc., we denoted the submatrices of the corresponding stiffness matrices $\mathbf{A}^i$ and $\mathbf{A}^j$ for the subregions $\Omega_i$ and $\Omega_j$, respectively. An index $\Gamma$, as in $\mathbf{A}_{1\Gamma}^i$ etc., indicates those submatrices which comprise finite elements belonging to the common boundary $\Gamma_{ij}$ between both subregions. This scheme holds for an arbitrary number of subregions $\Omega_i$, provided that all matrix systems $\mathbf{A}_i$ are properly reordered with regard to the displacements $\mathbf{u}_\Gamma^{ij}$ at the various common boundaries $\Gamma_{ij}$. As a result, the submatrices $\mathbf{A}_{11}^i$ etc. of each matrix $\mathbf{A}_i$ can be found in the global stiffness matrix $\mathbf{A}$ at entries corresponding to the global numbering scheme used for the unknown coefficients of $\mathbf{u}$.

To calculate the deformation of an anatomical structure given a set of spatial correspondences between images, these correspondences must be integrated into the linear equation system. To this end, we use the procedure described in Huebner *et al.* [22] and Peckar *et al.* [23]: Since a value for the unknown $u_j$ is given through the established correspondences, $u_j$ can be incorporated into the linear equation system by a subtraction of the product $u_j \mathbf{A}_j$, where $\mathbf{A}_j$ denotes the $j$-th column of the stiffness matrix $\mathbf{A}$, from the righthand side vector $\mathbf{b}$, followed by a substitution of the given value into the $j$-th row of $\mathbf{b}$. Thereafter, the $j$-th row and column of $\mathbf{A}$ are set to zero and, respectively, the diagonal element $A_{jj}$ to one. By repeating this procedure for a set of correspondences, e.g., to be defined at the surface of an anatomical structure, a direct mapping from the undeformed to the deformed state of the anatomical structure results. It follows from the construction scheme, that the given spatial correspondences are always exactly fulfilled, independent of the Lamé constant values used, or, in other words, the model automatically adjusts the necessary forces $\mathbf{f}$ and $\mathbf{g}$ [24], [25]. In principle, a correspondence can be given for each unknown. However, it is required that these correspondences should define a smooth vector field. Otherwise, violations of the underlying finite element mesh topology may arise and, as a consequence, locally incorrect deformations result.

Note, that the approach presented above is valid for 2D as well as 3D images. However, only 2D images will be considered below which is mainly due to a) huge storage requirements as well as high computing time in 3D and b) the lack of 3D implementations of the algorithms used for subregion segmentation and determination of the correspondences. In accordance with the underlying pixel grid of 2D images, we use four node quadrilateral finite elements, i.e. bilinear interpolation functions $\boldsymbol{\phi}_i$ to approximate $\mathbf{u}$ and $\mathbf{w}$. In 3D, trilinear finite elements with eight nodes could be used, resulting in linear interpolation functions. At the image border, homogeneous Dirichlet boundary conditions are assumed to force a preservation of the rectangular image border shape. All body forces like the gravity force were ignored due to the assumption of unknown, but static body forces. The resulting linear matrix system (9) is solved for the unknown displacements $\mathbf{u}$ by using the numerical method of conjugate gradients, e.g., [26].

## III. Material Parameters

By now, our implemented biomechanical model distinguishes two different materials, namely brain tissue and skull bone, which can be incorporated by assigning different values of the Lamé constants $\lambda$ and $\mu$ to the corresponding subregions. In order to use appropriate values for both materials, we carried out a comprehensive literature study summarized in Table I. Most of the values given there [16], [33], [34], [36] were taken from other reported values, mainly based on the works of Sauren and Classens [37] as well as Nagashima *et al.* [38]. Other authors [27], [28], [29], [30], [31], [35] incorporated real measured data, as reported by, e.g., McElhaney *et al.* [39] or Nahum *et al.* [40]. In our approach, where the deformations are driven by given correspondences which automatically adjust the forces, only the ratios between the values of $\lambda$ and $\mu$ are important. In Table II, the calculated ratios for the Lamé constant values given in Table I are summarized. Table II reveals the interesting fact that only a small number of different Lamé constant ratios for brain tissue and skull bone exists. Note, that the highly different ratios for brain tissue result from a small variation of the assumed Poisson's ratio $\nu$ (between $\nu = 0.48, \ldots, 0.499$), which defines the ratio between transverse contraction and longitudinal dilation.

To analyze the influence of varying the Lamé constant ratios on the deformation result, we performed several experiments using a $30 \times 30$ grid. In Figure 1, four parallel and equal correspondences were given while assuming here the calculated ratios for brain tissue, $\lambda/\mu = 24.0$, $\lambda/\mu = 49.0$, and $\lambda/\mu = 498.999$, respectively. The applied correspondences in all cases point in the direction of the lower right corner of the grid. As indicated by Figure 1, only slight differences in the deformations result. Using the ratios of skull bone instead, the same observation concerning the differences in the predicted deformations holds. Thus, we concluded from our experiments that the mean values of the ratios, namely $\lambda_{br}/\mu_{br} = 135.111$ and $\lambda_{sk}/\mu_{sk} = 0.718666$, may serve as valid estimates for the corresponding Lamé constant ratios.

For the simulation of different anatomical structures, we have to determine appropriate ratios for the Lamé constants between those structures. Following our previous practice for homogeneous materials, we calculated the ratios for the $\lambda$-values of skull bone and brain tissue and listed them in the last column of Table II. Here, a larger variability of the calculated ratios can be observed. How-

TABLE I

REPORTED VALUES OF THE LAMÉ CONSTANTS $\lambda$ AND $\mu$ FOR BRAIN TISSUE AND SKULL BONE. TADA *et al.*, TAKIZAWA *et al.*, AS WELL AS HARTMANN AND KRUGGEL DISTINGUISHED ORIGINALLY BETWEEN GREY MATTER AND WHITE MATTER, BUT HERE, ONLY THE VALUES FOR GREY MATTER ARE GIVEN. A BAR INDICATES THAT NO VALUES WERE GIVEN BY THE AUTHORS.

| material parameter values | brain | | skull | |
|---|---|---|---|---|
| article | $\lambda_{br}\,[kPa]$ | $\mu_{br}\,[kPa]$ | $\lambda_{sk}\,[kPa]$ | $\mu_{sk}\,[kPa]$ |
| Hosey and Liu 1982 [27] | 11101.8 | 22.2 | 1334570 | 1842980 |
| Ward 1982 [28] | 5270.3 | 219.6 | 1334570 | 1842980 |
| Ruan *et al.* 1991 [29] | 540.8 | 22.5 | 2093090 | 2663930 |
| Willinger *et al.* 1992 [30] | 5473.0 | 228.0 | 1388890 | 2083330 |
| Chu *et al.* 1994 [31] | 4110.7 | 83.9 | 1805560 | 2708330 |
| Tada *et al.* 1994 [16] | 8060.3 | 164.5 | 1466820 | 2025600 |
| Takizawa *et al.* 1994 [32] | 41.8 | 2.7 | - | - |
| Kuijpers *et al.* 1995 [33] | 8108.1 | 337.8 | 1805560 | 2708330 |
| Kumaresan and Radhakrisnan 1996 [34] | 540.8 | 22.5 | 1945000 | 2685950 |
| Whitman *et al.* 1996 [35] | - | - | 180556 | 270833 |
| Hartmann and Kruggel 1998 [36] | 12483.3 | 25.0 | 2093090 | 2663930 |

TABLE II

CALCULATED RATIOS FOR THE LAMÉ CONSTANTS FOR BRAIN AND SKULL TISSUE. ONLY THOSE PAPERS HAVE BEEN TAKEN INTO CONSIDERATION WHERE MATERIAL PARAMETER VALUES HAVE BEEN REPORTED FOR BOTH, BRAIN TISSUE AND SKULL BONE.

| ratios of the material parameter values | | | |
|---|---|---|---|
| article | $\lambda_{br}/\mu_{br}$ | $\lambda_{sk}/\mu_{sk}$ | $\lambda_{sk}/\lambda_{br}$ |
| Hosey and Liu 1982 [27] | 498.998 | 0.724 | 120.212 |
| Ward 1982 [28] | 24.0 | 0.724 | 253.226 |
| Ruan *et al.* 1991 [29] | 24.0 | 0.786 | 3870.28 |
| Willinger *et al.* 1992 [30] | 23.999 | 0.667 | 253.773 |
| Chu *et al.* 1994 [31] | 49.0 | 0.667 | 439.23 |
| Tada *et al.* 1994 [16] | 49.0 | 0.724 | 181.981 |
| Kuijpers *et al.* 1995 [33] | 24.0 | 0.667 | 222.686 |
| Kumaresan and Radhakrisnan 1996 [34] | 24.0 | 0.724 | 3596.45 |
| Hartmann and Kruggel 1998 [36] | 498.999 | 0.786 | 167.671 |

ever, it seems reasonable to choose again the mean value as ratio between the $\lambda$-values, namely $\lambda_{sk}/\lambda_{br} = 1011.72$, while keeping the internal Lamé constant ratios of each material constant. To demonstrate the influence of our determined Lamé constant values on the deformation result, four parallel and equal correspondences were again applied while assuming the various calculated ratios. As indicated by the resulting grid deformations and calculated displacement vector fields in Figure 2, the material parameter values for homogeneous skull bone result in a significant stiffer behaviour as compared to homogeneous brain tissue. By dividing the grid into two subregions $\Omega_1$ and $\Omega_2$, we obtain the result shown in Figure 2(c). In this case, the applied correspondences lead to a pure translation of the simulated bony rectangle which is surrounded by soft brain material. The corresponding displacement vector field in Figure 2(f) reveals, that the behaviour of the surrounding soft material is physically plausible: Along the path of translation, a stretching of the soft material occurs, while two vortices can be observed due to the lateral inflow of soft material.

## IV. EXPERIMENTS

As already mentioned above, our approach has been tested on 2D synthetic and tomographic datasets only, but the approach is also valid in 3D. However, for 3D images the subregion segmentation as well as the finding of correspondences is generally more difficult than for 2D images. Our approach has been implemented within the finite element programming environment DIFFPACK [41]. In the case of 2D images we applied a snake algorithm [42] for correspondence finding, whereas in 3D it seems promising to use deformable models for the purpose of determining the correspondences [43]. The synthetic experiments carried out comprised different types of movements (translation, rotation) and affine transformations (scaling, shearing) of a rigid object, embedded into elastic material. Figure 3 depicts the deformation results for different types of translations. In both cases, the star-shaped object remains perfectly rigid while the surrounding soft material is deformed. Note that the visual impression of the broadening of the grid lines can be traced back to our resampling process. Some problems arise for the case of objects rotated by an

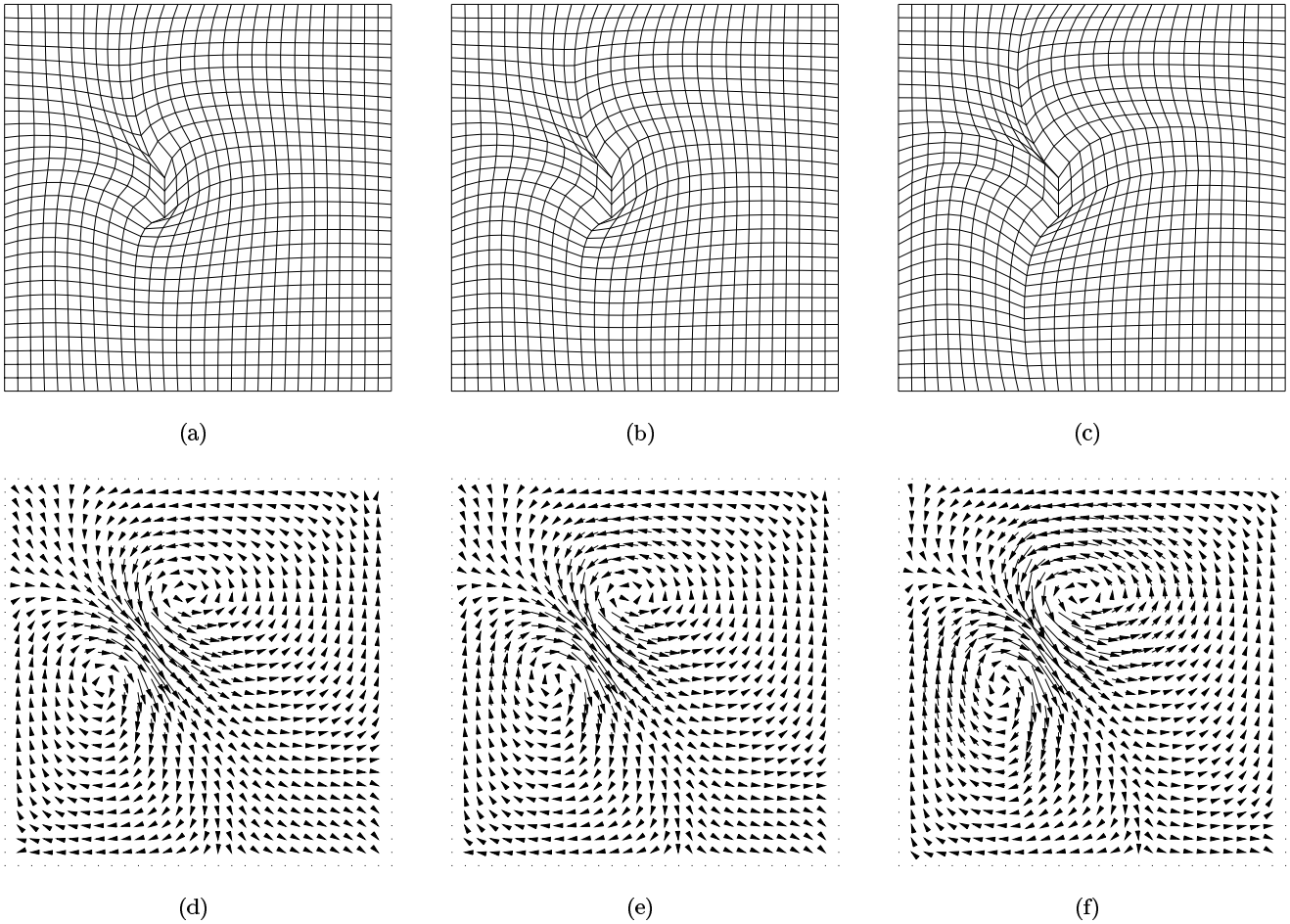


Fig. 1. To investigate the influence of different Lamé constant ratios, we compared the deformations of homogeneous brain tissue. Four parallel and equal correspondences, given in the upper left part of a $30 \times 30$ grid, were applied. The calculated grid deformations (top row) and displacement vector fields (bottom row) for brain tissue parameter values of $\lambda/\mu = 24.0$, $\lambda/\mu = 49.0$, and $\lambda/\mu = 498.999$ (from left to right) show only small differences.

angle larger than 45°, see Figure 4. A possible explanation might be that the linear elasticity assumption of small deformations is violated for large rotation angles.

For the experiments with real data, we used pre- and postoperative MR images which were routinely acquired in conjunction with the planning and radiological control of a tumor resection. The 2D images are corresponding slices of 3D datasets which were aligned by a rigid registration using 34 manually determined landmarks prior to our experiments. Due to the lack of appropriate intraoperative image data, a postoperative image was used to simulate an intraoperative one. First, the corresponding tumor and resection area outlines in both images were manually determined by a medical expert as indicated in Figures 5(a) and (b) by the white outlines. Thereafter, a snake algorithm [42] was applied to determine 618 correspondences for these outlines, which then were used as input to our model for the purpose of matching the pre- with the postoperative image. In a real clinical application, other input data like the insertion depth of surgical instruments could be used instead as correspondences. Figure 6(a) shows a locally erroneous registration result since homogeneous soft material for the whole image was only assumed. Note that local errors are clearly visible, especially in the vicinity of the ventricular system (see also the enlarged part of the ventricular system depicted in Figure 8(a)).

In order to improve this registration result, different materials were incorporated by assigning spatially different Lamé constants $\lambda$ and $\mu$ in accordance with the underlying anatomical structures. To this end, the preoperative image was segmented with a 2D interactive watershed algorithm [44] into four different regions, shown in Figure 5(c): combined skin/skull region (white), brain (dark grey), CSF (light grey), and surrounding air, i.e. image background (black). The air in the frontal sinus of the skull bone was assigned to the skull bone region since Hooke's law does not describe the physical behavior of air. Intracranial air and subarachnoidal CSF spaces between skull and brain were assigned to the brain tissue region, resulting in a rather simplified border between brain tissue and skull bone. But due to the viscosity of fluids like CSF, the applied compatibility boundary condition seems to be valid [45]. For brain tissue and skull bone, the previously determined ratios were used, while CSF and air were roughly approxi-

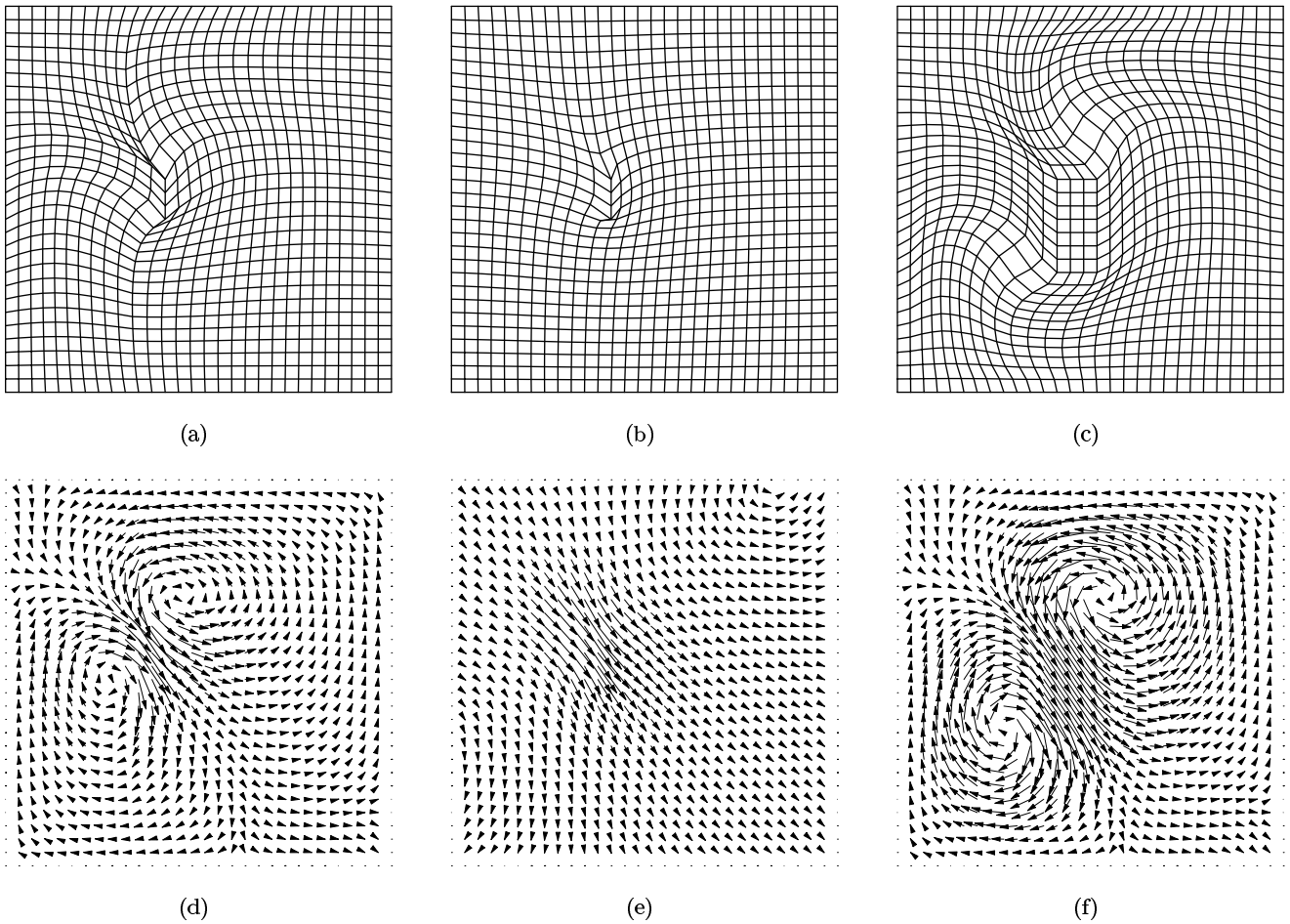


Fig. 2. Resulting grid deformation (top row) and displacement vector field (bottom row) while simulating different materials. In (a) and (b), homogeneous areas resembling brain tissue and skull bone were assumed, respectively. As expected, the skull-like material shows a much stiffer behaviour. By spatially different Lamé constant ratios, we can combine different materials as shown in (c). Here, a (simulated bone-like) rectangle embedded in simulated brain tissue results in a pure translation of the rectangle.

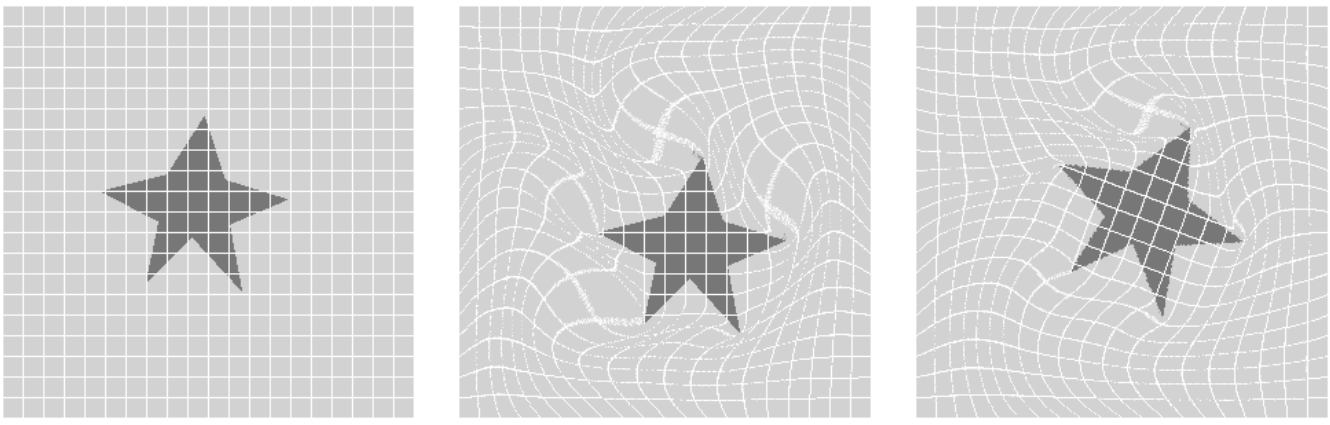


Fig. 3. Predicted translation of a rigid star embedded into soft material (a) due to two given correspondences (b). In (c), only one correspondence was used, resulting in a translation and rotation of the star.

mated as rigid and very soft materials, respectively. The material properties can be assigned to the finite element mesh, by a direct mapping of each pixel (or voxel in 3D) to the center of a finite element. Using four node quadrilateral finite elements, this results in $2(N+1)^2$ degrees of freedom for a 2D image with $N \times N$ pixels. In our concrete case of a $256 \times 256$ image, this mapping results in a matrix system containing 132098 degrees of freedom which is solved

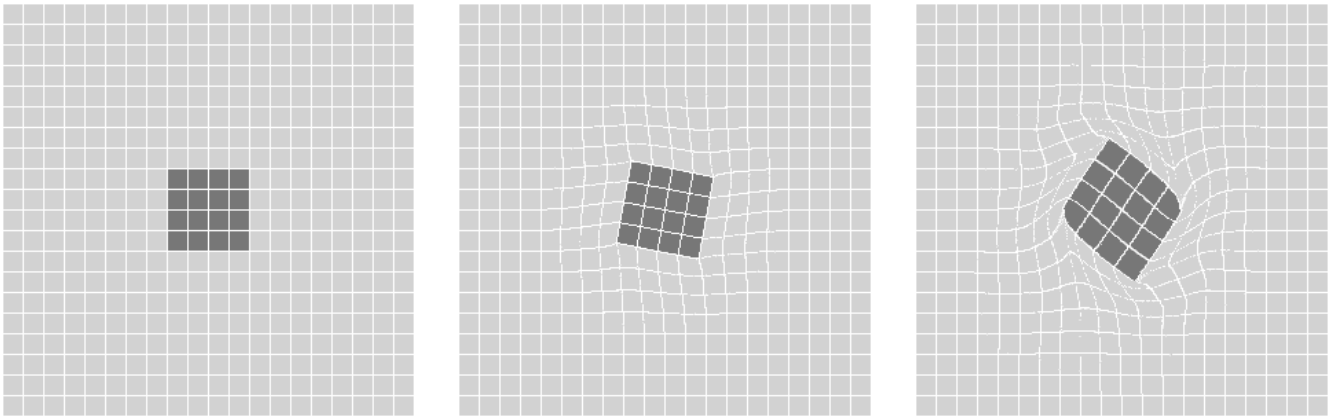

(a) (b) (c)

Fig. 4. Predicted clockwise rotation of a rigid block embedded into soft material (a). The rotation angles were 10° and 45° in subfigures (b) and (c), respectively. In (c), the approach starts to fail as can be seen by the deformation of the overlaid grid lines inside the rigid block.

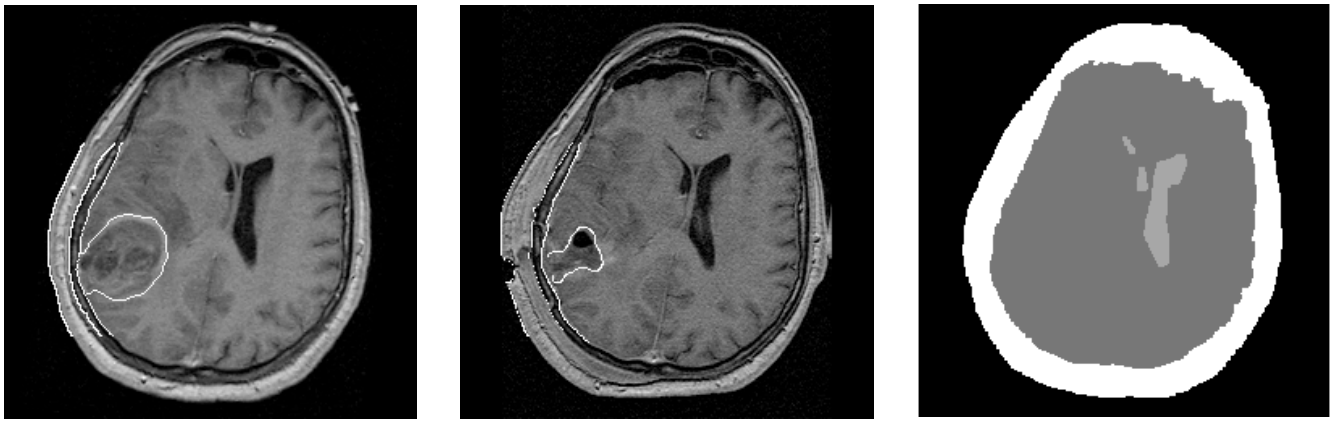

(a) (b) (c)

Fig. 5. Manually determined outlines in the pre- (a) and postoperative (b) image. In (c), the subregions as segmented with an interactive 2D watershed algorithm are depicted.

in the current, non-optimized implementation in about 45 minutes on a Sun ultra 2/1300 with 300 MHz. To transform the preoperative image, we use bilinear interpolation for both, the calculated displacement vector field and the image intensity function.

The registration result is shown in Figure 6(d). Here, a global movement of the head, forced by the given correspondences, can be observed which leads to a surprisingly poor registration result. Nevertheless, the assumption of inhomogeneous material properties leads to a completely different deformation behaviour as shown in the section of the displacement vector field in Figure 6(f). According to the rigid material assumption, the ventricular system cannot deform here thus leading to a small rotation of the whole ventricular system with respect to the postoperative image, best seen in the enlarged section depicted in Figure 8(b). As indicated by the corresponding grid deformation in Figure 6(e), there is a global movement of the head. This movement can be suppressed by preventing a deformation of the image background, i.e. by using the Lamé constant ratio of a rigid body for the image background, see Figures 7(a)-(c). In this case, an overall good registration result can be achieved, even in the vicinity of the ventricular system, as clearly depicted in Figure 8(c). Note, that no correspondences were given at the ventricular system, only the assumed inhomogeneous material properties suppress the deformation of the ventricular system.

However, a consideration of the results shown in Figures 6(a), 6(d), and 7(a) reveals a significant shift of the midline in the posterior half of the brain which is in contrast to the postoperative image 5(b) (see also [2]). This shift can be suppressed by using additional correspondences at the posterior midline (in this case, we used 68 manually determined correspondences) thus giving the result shown in Figure 7(d). Here, an overall good registration result is achieved and no shift of the posterior midline occurs, see the enlarged sections in Figure 9 for a comparison of the posterior midlines. As indicated by the corresponding grid deformations in Figures 7(e) and (b), the additionally applied correspondences significantly suppress the defor-

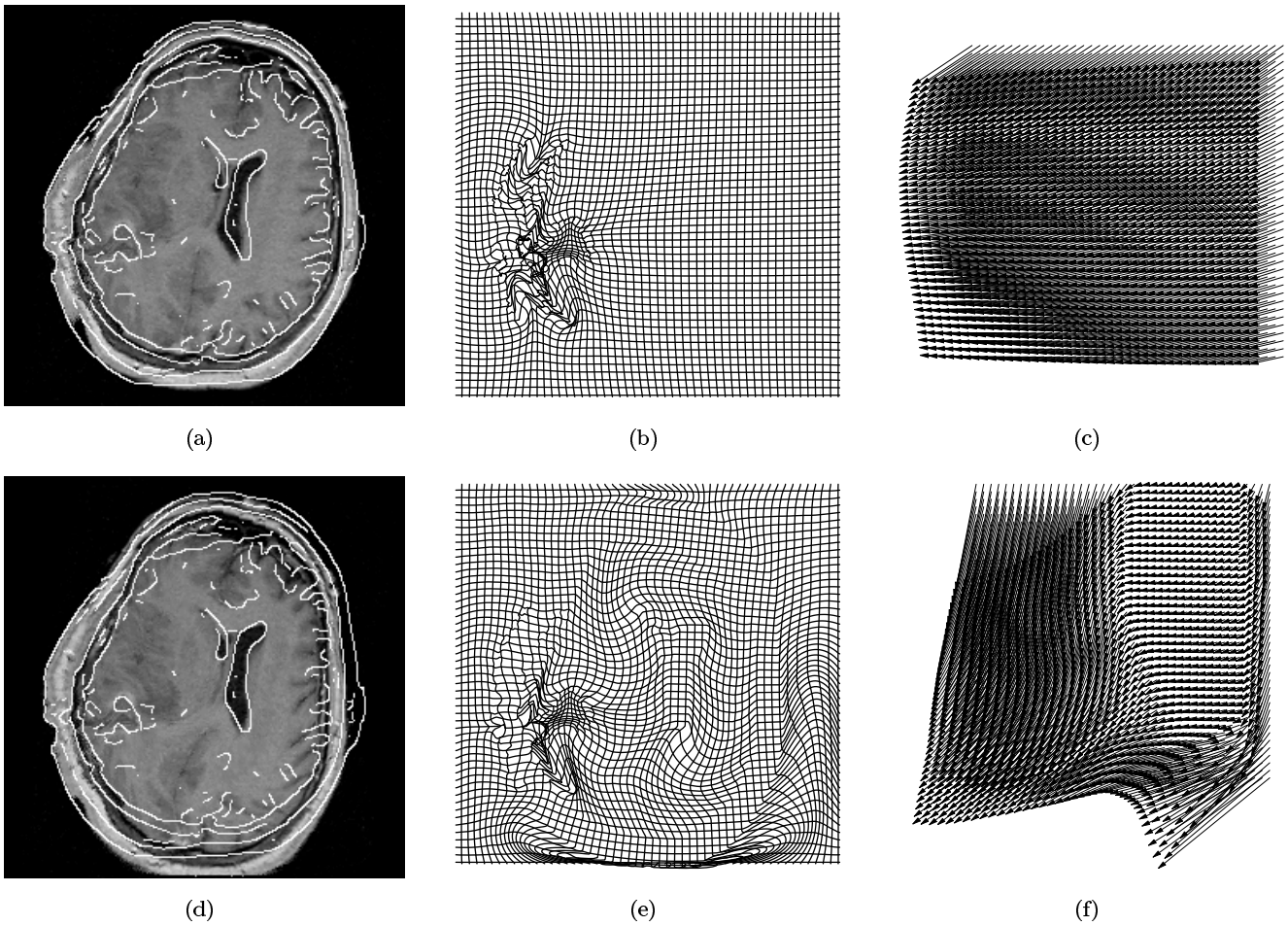


Fig. 6. Top row: (a) registration result assuming homogeneous soft material properties for the whole image (with overlaid Canny edges of the original postoperative image), (b) resulting grid deformation after application of the calculated displacement vector field, and (c) section of the displacement vector field from the bottom part of the ventricular system. Bottom row: based on the segmentation given in Figure 5(c), inhomogeneous material properties in conjunction with a soft image background are assumed.

mations in the left hemisphere. Only between the top end of the posterior midline and the ventricular system deformations occur due to the deformation of the elastic brain tissue, see Figure 7(f).

So far, the brain shift appearing in the upper left part of the postoperative image is not predicted by our biomechanical model, because the applied physical material description does not cope with the creation of new phenomena. But the underlying framework seems flexible enough to to deal with such situations by either introducing appropriate physical descriptions or modifying the underlying finite element mesh.

## V. Summary and Conclusion

We proposed a novel biomechanical model of the human head based on linear elasticity theory to predict brain deformations due to surgical interventions. The model is driven by a set of given correspondences, which are always exactly fulfilled, and allows to incorporates different material properties. Appropriate material parameter values were determined from the literature and have been experimentally validated. By carrying out experiments using 2D synthetic as well as real medical images, it turns out that the approach yields physically plausible deformation results. The incorporation of anatomical structures with different material properties leads to a significant improvement of the registration result for real MR images. In particular, we have shown that we can successfully suppress an unrealistic shift of the posterior brain midline by application of additional correspondences at this structure. Nevertheless, problems may arise in situations when other new phenomena have to be taken into consideration, like the occurrence of air in the cranium or perifocal edema. But we believe that the underlying framework seems flexible enough to cope with such phenomena. For example, to predict the brain shift at the top of the postoperative image in Figure 5(b), it seems promising to allow a tearing of the finite element mesh. We furthermore expect that the incorporation of different constitutive equations, like the Navier-Poisson law for an appropriate physical simulation

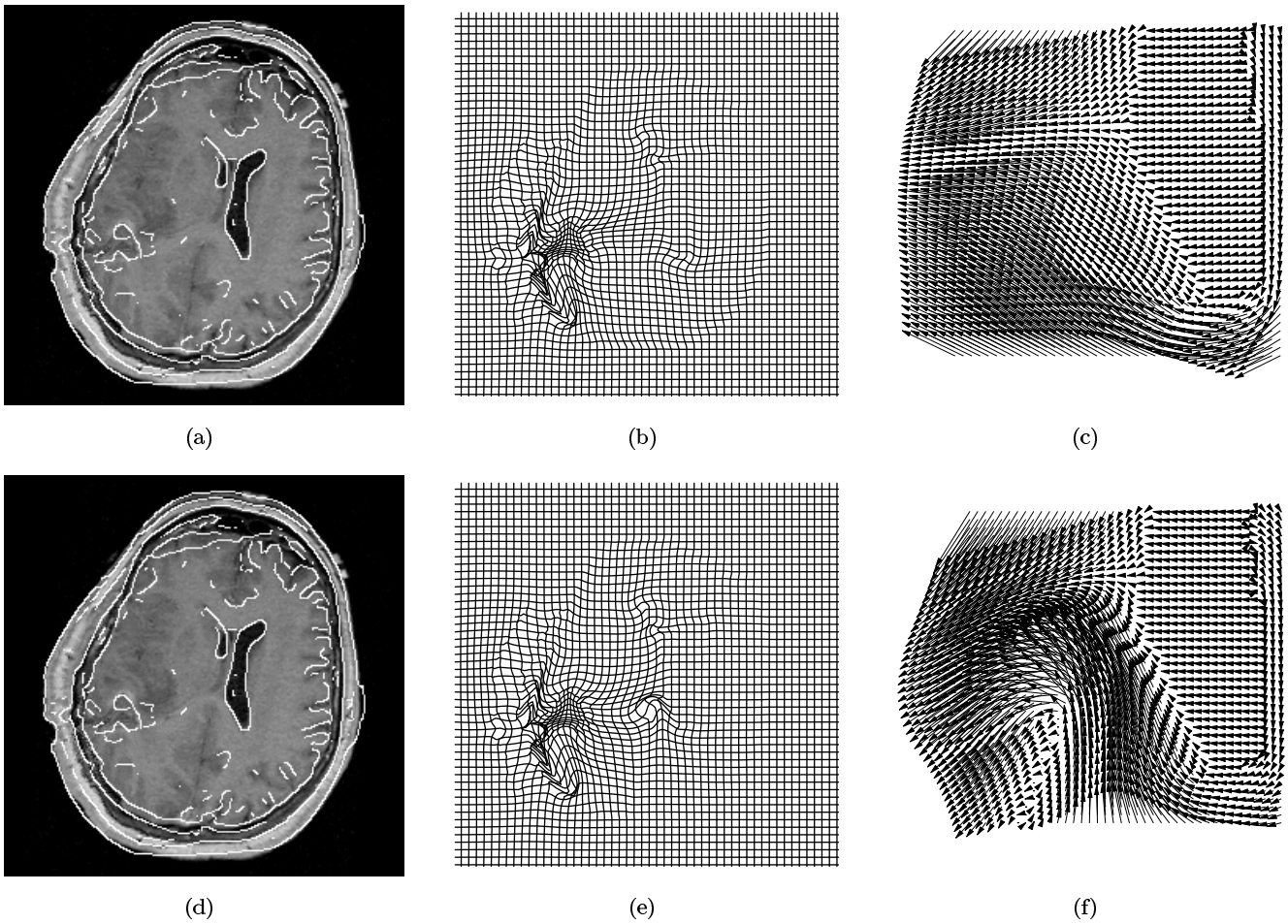


Fig. 7. Same as Figure 6(d), (e), (f) but assuming a rigid image background (top row) plus additionally 68 correspondences given at the midline in the posterior half of the brain (bottom row).

of CSF or more advanced constitutive equations for brain tissue [13], [8], [18], lead to further improvements of the prediction results. Besides the compatibility and equilibrium conditions used in our approach, additional boundary conditions, like the *no penetration boundary condition* for fluids [45], will be build into our computational scheme to take further physical properties into account.

As pointed out above, the processing time on a Sun ultra 2/1300 with 300 MHz are about 45 minutes, but the current implementation has a large potential for acceleration. For example, taking advantage of the symmetry of the stiffness matrix $\mathbf{A}$ will cut down the processing times and the memory space to a half. The use of anisotropic finite element meshes for the purpose of reducing the number of degrees of freedom as well as of more sophisticated preconditioners will further significantly reduce the processing time. A 3D extension of the implementation is under work.

## VI. Acknowledgement

Support of Philips Research Laboratories Hamburg, project IMAGINE (IMage- and Atlas-Guided Interventions in NEurosurgery), is gratefully acknowledged. We thank the anonymous reviewers for their constructive comments.

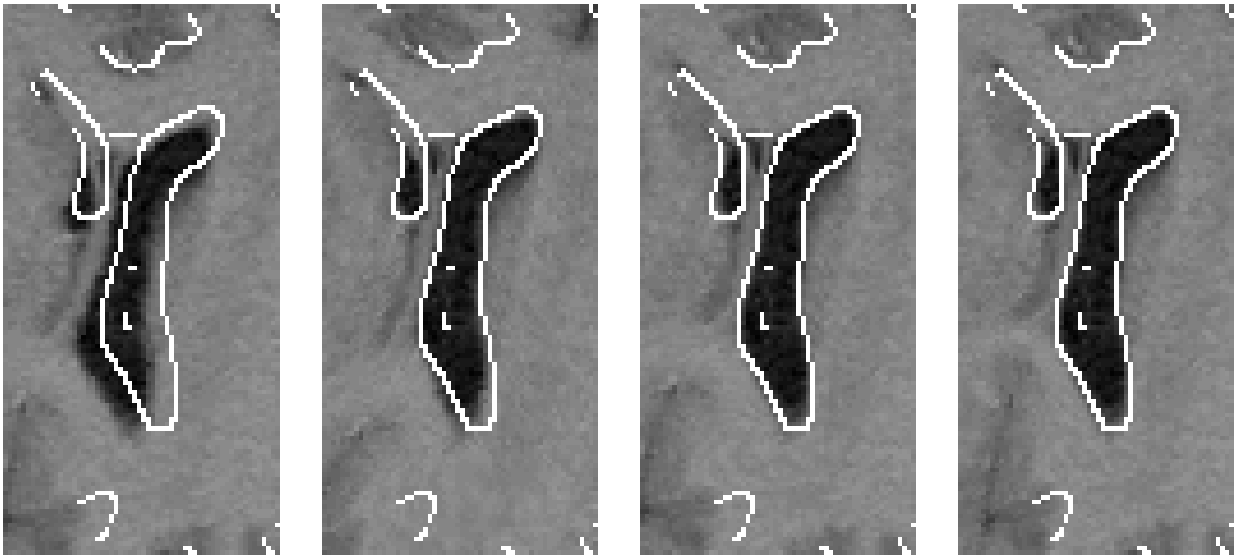

(a) (b) (c) (d)

Fig. 8. Enlarged parts of the ventricular systems of Figures 6(a), 6(d), 7(a), and 7(d) with overlaid Canny edges of the original postoperative image. Subfigure (a) shows the result for homogeneous soft material, (b) for the inhomogeneous case, (c) for the inhomogeneous case with rigid image background, and (d) for the case with additional 68 correspondences.

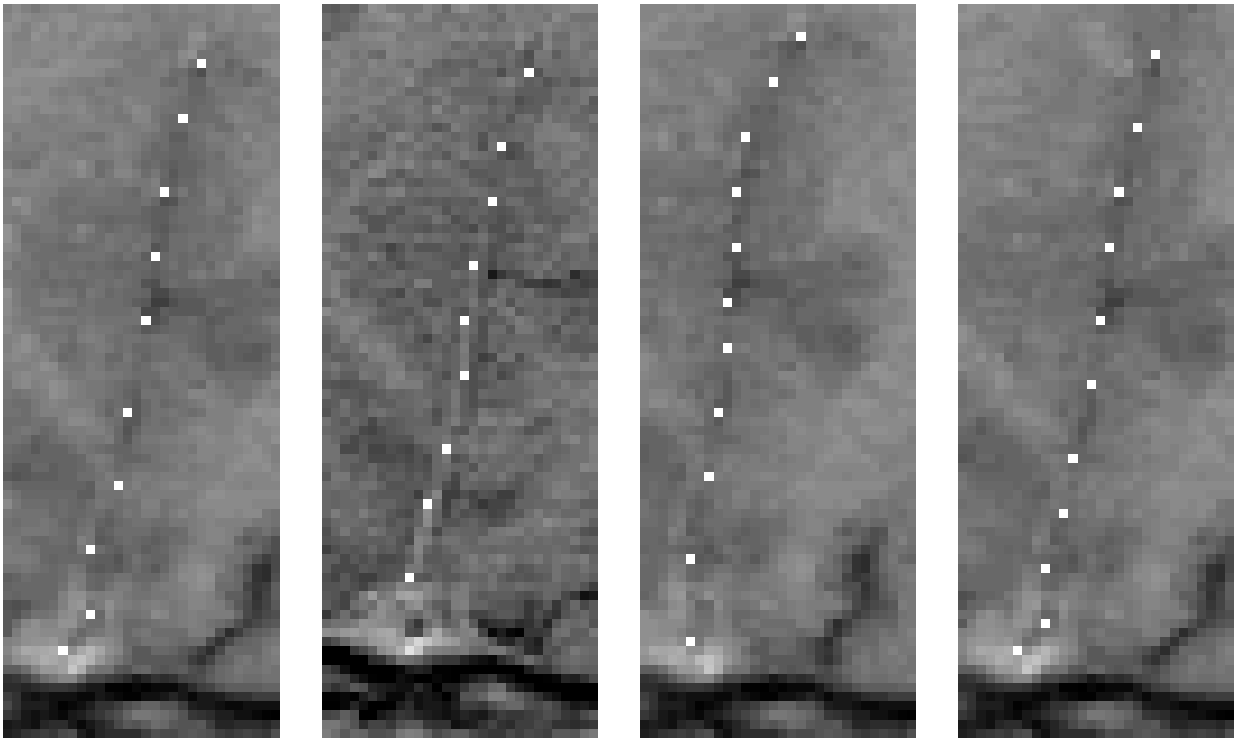

(a) (b) (c) (d)

Fig. 9. Enlarged parts of the posterior midline from a) the preoperative image, b) the postoperative image, c) the image in Figure 7(a) with inhomogeneous material properties, and d) the image in Figure 7(d) with inhomogeneous materials and additional correspondences given at the posterior midline. For visualization purposes, we manually marked the posterior line with white squares. A comparison with the pre- and postoperative images reveals, that in (c) larger deviations are visible while in (d) no shift of the midline occurs.

## References


[1] D. L. G. Hill, C. R. Maurer, R. J. Maciunas, J. A. Barwise, J. M. Fitzpatrick, and M. Y. Wang, "Measurement of Intraoperative Brain Surface Deformation under a Craniotomy," *Neurosurgery*, vol. 43, no. 3, pp. 514–526, September 1998.

[2] C. R. Maurer, D. L. G. Hill, A. J. Martin, H. Liu, McCue M., D. Rueckert, D. Lloret, W. A. Hall, R. E. Maxwell, D. J. Hawkes, and C. L. Truwit, "Investigation of Intraoperative Brain Deformation Using a 1.5-T Interventional MR System: Preliminary Results," *IEEE Transactions on Medical Imaging*, vol. 17, no. 5, pp. 817–825, October 1998.

[3] R. D. Bucholz, D. D. Yeh, J. Trobaugh, L. L. McDurmont, C. Sturm, C. Baumann, J. M. Henderson, A. Levy, and P. Kessman, "The Correction of Stereotactic Inaccuracy Caused by Brain Shift Using an Intraoperative Ultrasound Device," in *Computer Vision, Virtual Reality and Robotics in Medicine and Medical Robotics and Computer-Assisted Surgery (CVRMed-MRCAS'97)*, J. Troccaz, E. Grimson, and R. Mösges, Eds., Grenoble, France, 1997, vol. 1205 of *Lecture Notes in Computer Science*, pp. 459–466, Springer Verlag.

[4] P. J. Edwards, D. L. G. Hill, J. A. Little, and D. J. Hawkes, "A three-component deformation model for image-guided surgery," *Medical Image Analysis*, vol. 2, no. 4, pp. 355–367, 1998.

[5] C. Davatzikos, "Nonlinear Registration of Brain Images Using Deformable Models," in *Proceedings of the IEEE Workshop on Mathematical Methods in Biomedical Image Analysis*, M. E. Kavanaugh, Ed., San Francisco, USA, June 1996, pp. 94–103.

[6] S. K. Kyriacou and C. Davatzikos, "A Biomechanical Model of Soft Tissue Deformation, with Applications to Non-rigid Registration of Brain Images with Tumor Pathology," in *Medical Image Computing and Computer-Assisted Intervention (MICCAI'98)*, W. M. Wells, A. Colchester, and S. Delp, Eds. October 1998, number 1496 in Lecture Notes in Computer Science, pp. 531–538, Springer Verlag.

[7] M. Mooney, "A Theory of Large Elastic Deformation," *Journal of Applied Physics*, vol. 11, pp. 582–592, September 1940.

[8] K. K. Mendis, R. L. Stalnaker, and S. H Advani, "A Constitutive Relationship for Large Deformation Finite Element Modeling of Brain Tissue," *Journal of Biomechanical Engineering*, vol. 117, pp. 279–285, August 1995.

[9] W. Maurel, Y. Wu, N. Magnenat Thalmann, and D. Thalmann, *Biomechanical Models for Soft Tissue Simulation*, Basic Research Series. Springer Verlag, 1998.

[10] M. S. Estes and J. H. McElhaney, "Response of Brain Tissue to Compressive Loading," *American Society of Mechanical Engineers*, vol. 70-BHF-13, pp. 1–4, 1970.

[11] H. Lester, S. R. Arridge, and K. M. Jansons, "Local deformation metrics and nonlinear registration using a fluid model with variable viscosity," in *Proceedings of the Medical Image Understanding and Analysis (MIUA'98), Leeds, UK*, E. Berry, D. Hogg, K. V. Mardia, and M. A. Smith, Eds. July 1998, pp. 44–48, University of Leeds.

[12] O. Škrinjar, D. Spencer, and J. Duncan, "Brain Shift Modeling for Use in Neurosurgery," in *Medical Image Computing and Computer-Assisted Intervention (MICCAI'98)*, W. M. Wells, A. Colchester, and S. Delp, Eds. October 1998, number 1496 in Lecture Notes in Computer Science, pp. 641–648, Springer Verlag.

[13] M. R. Pamidi and S. H. Advani, "Nonlinear Constitutive Relations for Human Brain Tissue," *Journal of Biomechanical Engineering*, vol. 100, pp. 44–48, 1978.

[14] Y. C. Fung, *Biomechanics: Mechanical Properties of Living Tissues*, Springer-Verlag, 1993.

[15] K. D. Paulsen, M. I. Miga, F. E. Kennedy, P. J. Hoopes, A. Hartov, and D. W. Roberts, "A Computational Model for Tracking Subsurface Tissue Deformation During Stereotactic Neurosurgery," *IEEE Transactions on Biomedical Engineering*, vol. 46, no. 2, pp. 213–225, February 1999.

[16] Y. Tada, T. Nagashima, and M. Takada, "Biomechanics of brain tissue (simulation of cerebrospinal fluid flow)," *JSME International Journal, Series A (Mechanics and Material Engineering)*, vol. 37, no. 2, pp. 188–194, April 1994.

[17] A. Hagemann, K. Rohr, H. S. Stiehl, U. Spetzger, and J. M. Gilsbach, "Nonrigid matching of tomographic images based on a biomechanical model of the human head," in *Medical Imaging 1999 – Image Processing (MI'99)*, K. Hanson, Ed., San Diego, USA, February 1999, Proceedings of the SPIE International Symposium, pp. 583–592.

[18] K. Miller and K. Chinzei, "Constitutive modelling of brain tissue: Experiment and theory," *Journal of Biomechanics*, vol. 30, pp. 1115–1121, 1997.

[19] E. K. Walsh and A. Schettini, "Brain tissue elasticity and CSF elastance," *Neurological Research*, vol. 12, pp. 123–127, June 1990.

[20] C. Cuvelier, A. Segal, and A. A. van Steenhoven, *Finite Element Methods and Navier-Stokes Equations*, D. Reidel Publishing Company, 1986.

[21] H. Kardestuncer and D. H. Norrie, *Finite Element Handbook*, McGraw-Hill Company, 1987.

[22] K. H. Huebner, E. A. Thornton, and T. G. Byrom, *The Finite Element Method For Engineers*, John Wiley & Sons, 1995.

[23] W. Peckar, C. Schnörr, K. Rohr, and H. S. Stiehl, "Two-Step Parameter-Free Elastic Image Registration with Prescribed Point Displacements," *9th Int. Conf. on Image Analysis and Processing (ICIAP'97)*, vol. 1310, pp. 527–534, 1997.

[24] P. G. Ciarlet, *Mathematical Elasticity: Three-Dimensional Elasticity*, vol. 20 of *Studies in Mathematics and its Applications*, North-Holland, 1988.

[25] W. Peckar, *Application of Variational Methods to Elastic Registration of Medical Images*, Ph.D. thesis, Universität Hamburg, Fachbereich Informatik, AB KOGS, 1998.

[26] H. R. Schwarz, *Methode der Finiten Elemente*, Teubner Verlag, 1984.

[27] R. R. Hosey and Y. K. Liu, "A Homeomorphic Finite Element Model of the Human Head and Neck," in *Finite Elements in Biomechanics*, chapter 18, pp. 379–401. John Wiley & Sons, 1982.

[28] C. C. Ward, "Finite Element Models of the Head and Their Use in Brain Injury Research," in *Proceedings of 26th Stapp Car Crash Conference*, Ann Arbor, USA, 1982, pp. 71–85.

[29] J. S. Ruan, T. B. Khalil, and A. I. King, "Human Head Dynamic Response to Side Impact by Finite Element Modeling," *Journal of Biomechanical Engineering*, vol. 113, pp. 276–283, August 1991.

[30] R. Willinger, C. M. Kopp, and D. Césari, "New concept of contrecoup lesion mechanism: modal analysis of a finite element model of the head," *Proceedings on Int. Res. Council Biokinetics Impacts*, pp. 283–298, September 1992.

[31] C.-S. Chu, M.-S. Lin, H.-M. Huang, and Maw-Chang Lee, "Finite element analysis of cerebral contusion," *Journal of Biomechanics*, vol. 27, no. 2, pp. 187–194, February 1994.

[32] H. Takizawa, K. Sugiura, M. Baba, and J. D. Miller, "Analysis of Intracerebral Hematoma Shapes by Numerical Computer Simulation Using the Finite Element Method," *Neurologica Medico-Chirurgica*, vol. 34, no. 2, pp. 65–69, February 1994.

[33] A. H. Kuijpers, M. H. A. Claessens, and A. A. H. J. Sauren, "The Influence of Different Boundary Conditions on the Response of the Head to Impact: A Two-Dimensional Finite Element Study," *Journal of Neurotrauma*, vol. 12, no. 4, pp. 715–724, 1995.

[34] S. Kumaresan and S. Radhakrisnan, "Importance of partitioning membranes of the brain and the influence of the neck in head injury modelling," *Medical and Biological Engineering and Computing*, vol. 34, pp. 27–34, January 1996.

[35] T. A. Whitman, G. R. Wodicka, M. T. Morgan, and J. D. Bourland, "Measurement and Modeling of the Vibrational Response of the Ovine Head as it relates to Intracranial Pressure," in *Bridging Disciplines For Biomedicine*, Amsterdam, Netherlands, October 1996, 18th Annual International Conference of IEEE Engineering in Medicine and Biology Society.

[36] U. Hartmann and F. Kruggel, "Erste klinische Untersuchungen mit einem mechanischen Finite-Elemente-Modell des menschlichen Kopfes," in *Bildverarbeitung für die Medizin 1998*, T. Lehmann, V. Metzler, K. Spitzer, and T. Tolxdorff, Eds. March 1998, *Informatik aktuell*, pp. 59–63, Springer Verlag.

[37] A. A. H. J. Sauren and M. H. A. Claessens, "Finite element modeling of head impact: The second decade," in *Proceedings of the International IRCOBI, Conference on Biomechanics of Impact*, 1993, pp. 241–254.

[38] T. Nagashima, T. Shirakuni, and S. I. Rapoport, "A Two-Dimensional Finite Element Analysis of Vasogenic Brain Edema," *Neurologica Medico-Chirurgica.*, vol. 30, pp. 1, 1990.

[39] J. H. McElhaney, R. L. Stalnaker, and V. L. Roberts, "Biomechanical Aspects of Head Injury," *Human Impact Response*, pp. 85–112, 1973.

[40] A. M. Nahum, R. Smith, and C. C. Ward, "Intracranial Pressure Dynamics During Head Impact," in *Proceedings of 21st Stapp Car Crash Conference*, 1977, pp. 339–366.

[41] Numerical Objects AS, "Diffpack," http://www.nobjects.com/Diffpack/, 1999.

[42] Kass M., A. Witkin, and D. Terzopoulos, "Snakes: Active contour models," *International Journal of Computer Vision*, vol. 1, no. 4, pp. 321–331, 1988.
[43] T. McInerney and D. Terzopoulos, "Deformable Models in Medical Image Analysis: A Survey," *Medical Image Analysis*, vol. 1, no. 2, 1996.
[44] S. Tieck, S. Gerloff, and H. S. Stiehl, "Interactive graph-based editing of watershed-segmented 2D-images," in *Workshop on Interactive Segmentation of Medical Images (ISMI'98)*, University of Amsterdam, Dept. of Computer Science, Intelligent Sensory Information systems Research Group, September 1998, http://carol.wins.ura.nl/ silvia/workshop.
[45] Y. C. Fung, *A First Course In Continuum Mechanics*, Prentice-Hall, 1994.